Dalton Transactions

ROYAL SOCIETY OF CHEMISTRY

PAPER

View Article Online
View Journal | View Issue

Cite this: *Dalton Trans.*, 2024, **53**, 9862

Complexation and disproportionation of group 4 metal (alkoxy) halides with phosphine oxides†

Carlotta Seno, Rohan Pokratath, Ajmal Roshan Unniram Parambil, Dietger Van den Eynden, Evert Dhaene, Alessandro Prescimone and Jonathan De Roo *

Group 4 Lewis acids are well-known catalysts and precursors for (non-aqueous) sol–gel chemistry. Titanium, zirconium and hafnium halides, and alkoxy halides are precursors for the controlled synthesis of nanocrystals, often in the presence of Lewis base. Here, we investigate the interaction of Lewis bases with the tetrahalides (MX_4, X = Cl, Br) and metal alkoxy halides ($MX_x(OR)_{4-x}$, x = 1–3, R = O^{i}Pr, O^{t}Bu). The tetrahalides yield the expected Lewis acid–base adducts MX_4L_2 (L = tetrahydrofuran or phosphine oxide). The mixed alkoxy halides react with Lewis bases in a more complex way. ^{31}P NMR spectroscopy reveals that excess of phosphine oxide yields predominantly the complexation product, while a (sub)stoichiometric amount of phosphine oxide causes disproportionation of the $MX_x(OR)_{4-x}$ species into $MX_{x+1}(OR)_{3-x}$ and $MX_{x-1}(OR)_{5-x}$. The combination of complexation and disproportionation yields an atypical Job plot. In the case of zirconium isopropoxy chlorides, we fitted the concentration of all observed species and extracted thermodynamic descriptors from the Job plot. The complexation equilibrium constant decreases in the series: $ZrCl_3(O^iPr) > ZrCl_2(O^iPr)_2 \gg ZrCl(O^iPr)_3$, while the disproportionation equilibrium constant follows the opposite trend. Using calculations at the DFT level of theory, we show that disproportionation is driven by the more energetically favorable Lewis acid–base complex formed with the more acidic species. We also gain more insight into the isomerism of the complexes. The disproportionation reaction turns out to be a general phenomenon, for titanium, zirconium and hafnium, for chlorides and bromides, and for isopropoxides and *tert*-butoxides.

Received 2nd May 2024,
Accepted 3rd May 2024

DOI: 10.1039/d4dt01299b

rsc.li/dalton

1. Introduction

Lewis acids play an essential role in many catalytic and biological processes and understanding their interaction with Lewis bases has driven chemistry forward. Group 4 metals (Ti, Zr, Hf) produce an interesting class of Lewis acids, almost exclusively featuring the +IV oxidation state.[1] The metal halides are economical precursors for the synthesis of group 4 materials, ranging from amorphous gels,[2,3] to crystalline nanoparticles.[4–8] Given that the halides are often dissolved in alcohol or combined with metal alkoxides, the actual reactive species in solution are often mixed alkoxy halides.[9–11] In the synthesis of zirconia nanocrystals from zirconium chloride and zirconium isopropoxide, zirconium di-isopropoxy di-chloride is a confirmed intermediate, which interacts with the Lewis base present: tri-*n*-octylphosphine oxide (TOPO). The formed complex decomposes at 340 °C to zirconia nanocrystals.[11–13]

$$2ZrCl_2(O^iPr)_2(TOPO)_2 \rightarrow ZrCl_4 + ZrO_2 + 4TOPO + 2C_3H_6 + 2HO^iPr \quad (1)$$

The same chemistry is relevant for titania and hafnia nanocrystals, where the choice of metal halide, metal alkoxide, and of the Lewis base plays a crucial role in the determination of the final properties of the product.[4,14–18] Although the nature and stability of the formed metal complexes are of direct consequence to the outcome of nanocrystal syntheses, detailed insights into the coordination of alkoxy halides are lacking.

The metal halides were more extensively studied. All twelve possible MX_4 compounds are known, with M = Ti, Zr, Hf and X = F, Cl, Br, I.[1] All of them are strong Lewis acids. Some are monomeric molecules (*e.g.*, $TiCl_4$, $TiBr_4$ and TiI_4), while others form polymeric solids (TiF_4, $ZrCl_4$ and $HfCl_4$).[19–21] The polymeric structure consists of bridging halides, which increases

Department of Chemistry, University of Basel, Mattenstrasse 22, 4058 Basel, Switzerland. E-mail: Jonathan.DeRoo@unibas.ch

†Electronic supplementary information (ESI) available: Crystallographic data of previously unreported single crystals and their characterization with ^{1}H NMR and ^{31}P NMR, PXRD, IR and TGA. ^{1}H NMR and ^{31}P NMR spectra of metal complexes and detailed description of job plot analysis. CCDC 2219601, 2219602 and 2219604–2219606. The raw data for all the figures are openly available on Zenodo: **https://doi.org/10.5281/zenodo.11192035**. For ESI and crystallographic data in CIF or other electronic format see DOI: **https://doi.org/10.1039/d4dt01299b**

the coordination number. It is preferred for the larger metals (Zr/Hf) and/or smaller halides (F).[7] The metal halides react with Lewis bases (L), forming the MX_4L_2 adducts, with a coordination number of 6.[22] In case of titanium fluoride, the solution behavior is often complex with the ionic species $TiF_3L_3^+$ and $Ti_4F_{18}^{2-}$ present, next to TiF_4L_2.[22] Under-supply of Lewis base (*e.g.*, only one equivalent) further promotes ionization:

$$3TiF_4L \rightarrow TiF_3L_3^+ + Ti_2F_9^- \quad (2)$$

The isolated species in the solid state is usually *cis*-TiF_4L_2. A mixture of *trans*-TiF_4L_2 and *cis*-TiF_4L_2 complexes were found in solution in case the Lewis base was sufficiently steric. While triphenylphosphine oxide produces *cis*-TiF_4L_2 in the solid state, 2,6-dimethylpyridine-*N*-oxide produces the *trans* configuration. The *cis*/*trans* equilibrium was rationalized as follows.[23]

• Steric repulsion between halides favors the *trans* configuration

• Steric repulsion between the ligands favors the *trans* configuration

• To maximize halide-metal p_π–d_π bonding, the *cis* configuration is favored.

The last argument is justified by the shorter bond length of the halide *trans* to the Lewis base, compared to the two fluorides *trans* with respect to each other. The halide competes more effectively for the d_π with a neutral Lewis base than with another halide. While the above arguments were originally made for titanium fluoride, they explain a more general pattern in the literature.

The halide effect is apparent from the THF complexes of TiF_4 and $TiCl_4$. $TiF_4(THF)_2$ has the *cis* configuration,[24] but $TiCl_4(THF)_2$ is found both as *cis* and *trans*.[25,26] For a larger metal, the steric repulsion between the chloride ligands is mitigated, evidenced by the sole isolation of *cis*-$ZrCl_4(THF)_2$ and *cis*-$HfCl_4(THF)_2$.[27,28] Using tetramethylethylenediamine as bidentate Lewis base, *cis*-$ZrCl_4L_2$ was obtained and again, the Zr–Cl bond distances are longer for the two *trans* chloride ligands (2.43 Å) and shorter for the chloride ligands *trans* to the Lewis base (2.41 Å).[29] Acetonitrile (ACN) is a less steric ligand than THF and only *cis* configurations were determined for $TiCl_4(ACN)_2$,[30,31] $TiBr_4(ACN)_2$,[32] $ZrCl_4(ACN)_2$,[33,34] and $ZrBr_4(ACN)_2$.[35,36] On the other hand, tri-*n*-octylphosphine oxide is more sterically bulky than THF and favors the *trans* configuration for $ZrCl_4(R_3PO)_2$.[11]

Ligand exchange of Lewis bases bound to TiF_4 was shown to occur *via* a dissociative mechanism featuring an intermediate with coordination number of 5.[22,37,38] The kinetic stability of the complexes follows the order of Lewis base strength[39]

$$\begin{aligned}\text{pyridine} > Ph_3PO \approx Me_2SO > (MeO)_3PO \\ > Et_2O > MeCN\end{aligned} \quad (3)$$

Mixed alkoxy halide species are formed when a metal halide is mixed with a metal alkoxide.[2,40,41] The stoichiometry of the final product can be varied:

$$3MCl_4 + M(OR)_4 \rightarrow 4MCl_3(OR) \quad (4)$$

$$MCl_4 + M(OR)_4 \rightarrow 2MCl_2(OR)_2 \quad (5)$$

$$MCl_4 + 3M(OR)_4 \rightarrow 4MCl(OR)_3 \quad (6)$$

The mixed alkoxy chloride also forms by reacting the metal alkoxide with acetyl chloride.[42] The ester is formed as a by-product.

$$M(OR)_4 + x\text{RCOCl} \rightarrow MCl_x(OR)_{4-x} + x\text{RCOOR} \quad (7)$$

The distinction between the different $MCl_x(OR)_{4-x}$ complexes *via* ^{1}H NMR is highly challenging due to the complex structure of the resonances.[2,40] After complexation with phosphine oxides, the different species can be distinguished *via* ^{31}P NMR.[11] However, the Lewis acid behavior of these mixed halide alkoxides is largely unexplored.

Here, we gain insight into the interaction between group 4 $MCl_{4-x}(OR)_x$ Lewis acids (M = Ti, Zr or Hf) and phosphine oxide Lewis bases, relevant for nanocrystal syntheses. Focusing first on pure metal halides, we synthesize and analyze the structure of previously unreported $ZrBr_4(THF)_2$ and various $MX_4(TPPO)$ (TPPO = triphenylphosphine oxide, X = Cl or Br) complexes with single-crystal XRD. All obtained complexes feature the *trans* configuration of the Lewis bases. Second, we study the interaction of mixed isopropoxy chloride with tri-*n*-octylphosphine oxide using ^{31}P NMR spectroscopy. We observe both complexation and disproportionation reactions. The latter are especially prevalent at sub-stoichiometric amounts of Lewis base and this behavior highly complicates the Job plot. Focusing on the case of zirconium, we model the Job plot using a set of chemical equations (in COPASI[43]), thus extracting the equilibrium constants for both complexation and disproportionation. With decreasing Lewis acidity ($MCl_3(OR)$ > $MCl_2(OR)_2$ > $MCl(OR)_3$), we find a lower complexation constant but a higher propensity for disproportionation. We showed the generality of the disproportionation behavior for all three metals, for different halides and different alkoxides.

2. Results and discussion

2.1. Lewis base adducts of MCl_4

The Lewis base adducts of titanium tetrahalides are well-reported in the literature but zirconium and hafnium tetrahalides are less well-documented. For completion, we synthesized and crystallized *trans*-$ZrBr_4(THF)_2$, see Fig. 1. The bond distances are reported in Table S1,† together with selected structures from the literature. While $ZrCl_4(THF)_2$ is *cis*, $ZrBr_4(THF)_2$ has the *trans* configuration. The M–O bond distance is slightly shorter in $ZrBr_4(THF)_2$, which is likely due to the absence of steric repulsion between the two THF ligands since the same effect is observed for *cis*-$TiCl_4(THF)_2$ and *trans*-$TiCl_4(THF)_2$, see Table S1.†

We previously showed that phosphine oxides quantitatively displace THF from zirconium chloride.[11] Therefore, we synthesized the triphenylphosphine oxide (TPPO) complexes of

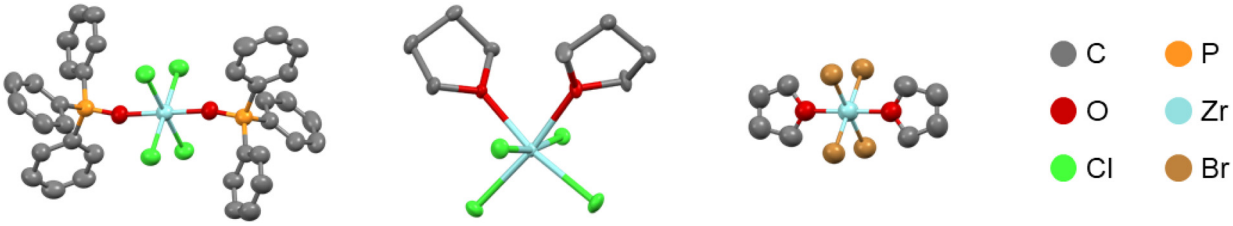

$ZrCl_4(TPPO)_2$ $ZrCl_4(THF)_2$ [40] $ZrBr_4(THF)_2$

Fig. 1 Structures of zirconium halide complexes determined by single-crystal XRD. The hydrogen atoms are omitted for clarity. Table S2† reports the resolved crystallographic parameters.

$ZrCl_4$, $ZrBr_4$ and $HfCl_4$ by ligand exchange from the THF complex and single-crystals were grown.

$$MX_4(THF)_2 + 2TPPO \rightarrow MX_4(TPPO)_2 + 2THF \quad (8)$$

Structural analysis *via* single-crystal XRD indicates that the TPPO complexes have the *trans* configuration, see Fig. 1 for the structure of *trans*-$ZrCl_4(TPPO)_2$ (the other structures are shown in Fig. S1†). Including literature data, we conclude that all TPPO adducts of zirconium and hafnium tetrahalides adopt the *trans* configuration (Table 1). Compared to the THF complexes, the TPPO complexes generally feature a longer M–X distance and a shorter M–O distance (Table S1†). This is a reflection of the higher Lewis basicity of phosphine oxides. In general, Table 1 follows the general trend laid out in the introduction. Larger halides and ligands promote the *trans* configuration. In addition, a larger metal size promotes the *cis* configuration as it allows to alleviate steric repulsion between the halides. A notable exception to this trend is the contrast between *cis*-$TiF_4(TPPO)_2$ and *trans*-$ZrF_4(TPPO)_2$. Even though the zirconium atom is larger than titanium, the configuration switches from *cis* to *trans*. We hypothesize that the energy difference between the fluorine p-orbitals and the zirconium d-orbitals is too high to allow for sufficient interaction, thereby removing the driving force for the *cis* configuration. All synthesized complexes were characterized by ^1H and ^{31}P NMR spectroscopy (Fig. S2†), thermogravimetric analysis (Table S3†) and infrared spectroscopy (Fig. S3†).

Table 1 Overview of *cis*/*trans* configuration in different group 4 metal halide complexes with either tetrahydrofuran (THF) or triphenylphosphine oxide (TPPO) as Lewis base

	THF	TPPO
TiF_4	*cis*[24]	*cis*[24]
$TiCl_4$	*cis*[25] and *trans*[26]	*trans*[a] [46]
ZrF_4	—	*trans*[47]
$ZrCl_4$	*cis*[27]	*trans*[a]
$ZrBr_4$	*trans*[a]	*trans*[a]
$HfCl_4$	*cis*[28]	*trans*[a]

[a] This work.

Powder XRD confirmed that the bulk material has the same structure as the single crystals (Fig. S4†). The triphenylphosphine oxide complexes are all poorly soluble in chloroform and effectively insoluble in benzene, but ligand exchange for tri-*n*-octylphosphine oxide (TOPO) generates soluble complexes, with ^{31}P NMR shifts consistent with previous assignments (Fig. S5–S7†).[11] $TiCl_4(TOPO)_2$ appears as a sharp singlet at 77.4 ppm, $ZrCl_4(TOPO)_2$ at 72.9 ppm and $HfCl_4(TOPO)_2$ at 73.0 ppm. The Gutmann-Beckett method ranks the effective Lewis acidity by the ^{31}P NMR shift of triethylphosphine oxide (TEPO) bound to a Lewis acid.[44,45] A high chemical shift is related to a high effective Lewis acidity. Given the similar structure of TEPO and TOPO, we conclude that $TiCl_4$ has a higher effective Lewis acidity than $ZrCl_4$ and $HfCl_4$. The latter two have about the same effective Lewis acidity.

2.2. Complexation and disproportionation of $ZrCl_x(O^iPr)_{4-x}$

We synthesized three $ZrCl_x(O^iPr)_{4-x}$ (x = 1–3) compounds by reacting $Zr(O^iPr)_4.{}^iPrOH$ with acetylchloride in the correct ratios, see eqn (7). We then added an excess (4 equivalents) of TOPO to each compound to assess the complexation behavior. In case of $MCl_3(O^iPr)$, the ^{31}P NMR spectrum (Fig. 2A) shows one main signal for $MCl_3(O^iPr)(TOPO)_2$. In the case of $MCl_2(O^iPr)_2$, we observe two resonances pertaining to 2 isomers, see further details in the computational section. In case of $MCl(O^iPr)_3$, we observe a less intense signal for the $MCl(O^iPr)_3(TOPO)_2$ complex and also the resonances of the two $MCl_2(O^iPr)_2(TOPO)_2$ isomers are present. Based on the assignment and the positions in ^{31}P NMR spectrum, the effective Lewis acidity is ranked: $ZrCl_4$ > $ZrCl_3(O^iPr)$ > $ZrCl_2(O^iPr)_2$ > $ZrCl(O^iPr)_3$.

When only 1 equivalent of TOPO is added, the speciation changes, see Fig. 2B. Starting from $MCl_3(O^iPr)$, we detect $MCl_4(TOPO)_2$ as the main species in the ^{31}P NMR spectrum. For $MCl_2(O^iPr)_2$, we retrieve mostly $MCl_3(O^iPr)(TOPO)_2$ and for $MCl(O^iPr)_3$, we find almost exclusively the two isomers of $MCl_2(O^iPr)_2(TOPO)_2$. Note that species, which are not coordinated by TOPO, are not detected by ^{31}P NMR. To explain the data, we hypothesize a disproportionation reaction and formation of the stronger Lewis acid–base adduct. Take the example of $ZrCl_3(O^iPr)$. The reaction with 1 equivalent of

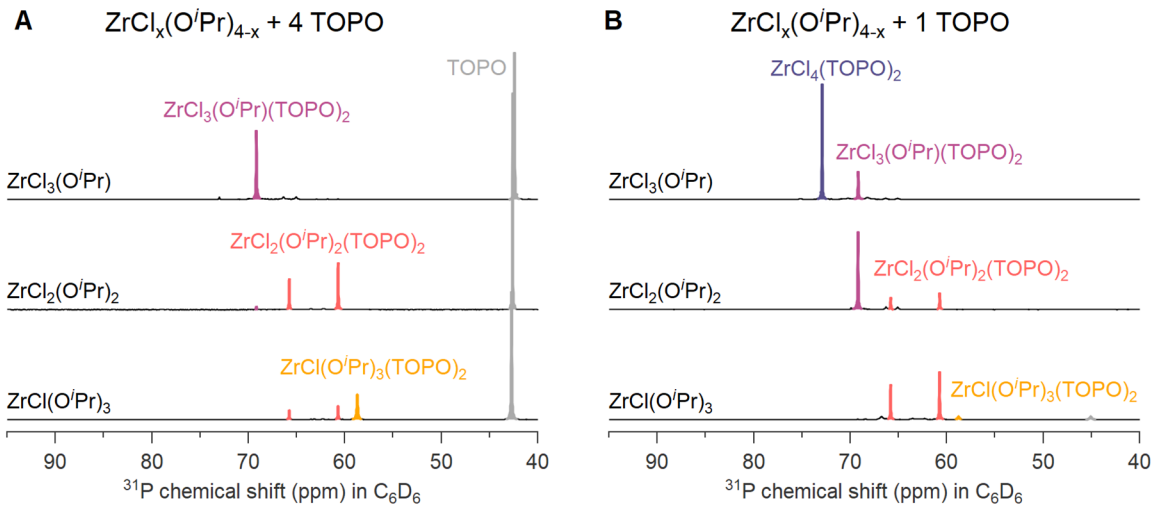

Fig. 2 ^{31}P NMR spectra at room temperature of zirconium alkoxy chloride complexes MCl$_x$(O^{i}Pr)$_{4-x}$ in benzene-d$_6$ with either (A) 4 equivalents or (B) 1 equivalent of TOPO. The concentration of zirconium is 0.05 M when mixed with 4 equivalents, and 0.125 M with 1 equivalent.

TOPO can be split in a disproportionation (eqn (9)) and a complexation reaction (eqn (10)):

$$\mathrm{ZrCl_3(OR)} \rightleftharpoons 0.5\mathrm{ZrCl_4} + 0.5\mathrm{ZrCl_2(OR)_2} \quad (9)$$

$$0.5\mathrm{ZrCl_4} + \mathrm{TOPO} \rightleftharpoons 0.5\mathrm{ZrCl_4(TOPO)_2} \quad (10)$$

Giving the total:

$$\mathrm{ZrCl_3(OR)} + \mathrm{TOPO} \rightleftharpoons 0.5\mathrm{ZrCl_4(TOPO)_2} + 0.5\mathrm{ZrCl_2(OR)_2} \quad (11)$$

After disproportionation, the Lewis base forms an adduct with the most Lewis acidic species, $ZrCl_4$. Hence, $ZrCl_4(TOPO)_2$ is detected in NMR, while $ZrCl_2(OR)_2$ is undetectable by ^{31}P NMR. In the absence of a disproportionation, complexation could only result in either 1 equivalent of $ZrCl_3(OR)(TOPO)$ or in 0.5 equiv. $ZrCl_3(OR)(TOPO)_2$ and 0.5 equiv. $ZrCl_3(OR)$. We thus assign the driving force of the disproportionation to the formation of stronger Lewis acid–base adduct; $ZrCl_4(TOPO)_2$. When supplying an excess of Lewis base, the disproportionation pathway is suppressed, the extent of which depends on the alkoxy chloride. For the case of MCl(O^{i}Pr)$_3$, the MCl$_2$(O^{i}Pr)$_2$(TOPO)$_2$ isomers (*i.e.*, the disproportionation product) were still significantly present at 4 equivalents of TOPO, see Fig. 2A.

There is no literature precedent for ligand-induced disproportionation in group 4. However, $TiCl_3(OMe)$ disproportionates upon heating and cannot be purified by distillation:[48]

$$2\mathrm{TiCl_3(OMe)} \xrightarrow{\text{heat}} \mathrm{TiCl_2(OMe)_2} + \mathrm{TiCl_4} \quad (12)$$

Precedent for ligand-induced disproportionation is found in group 13. Wiberg and coworkers reported in 1935 that BCl$_x$(OR)$_{3-x}$ species disproportionate into BCl$_{x+1}$(OR)$_{3-x-1}$ and BCl$_{x-1}$(OR)$_{3-x+1}$ (with x = 1, 2) when trimethylamine or an ether is introduced.[49,50] A quantitative analysis of the phenomenon was not reported.

2.3. Quantitative fit of the Job plot

Job plots are a popular technique to determine the stoichiometry of binding events.[51–54] In such a plot, the relative mole fraction of reagents is varied while keeping the sum of the concentrations constant. In case of zirconium isopropoxy chlorides interacting with TOPO, the Job plot becomes highly complicated since the reaction is not limited to complexation but also features disproportionation, see Fig. 3.

To quantify the disproportionation observed in the previous section, we modeled the Job plots with a series of equilibrium reactions. For the case of ZrCl$_3$(O^{i}Pr), we take a set of three equilibria, composed of a complexation (eqn (13)), a disproportionation (eqn (14)) and a decomplexation equilibrium (eqn (15)), where L = TOPO.

$$\mathrm{ZrCl_3(OR)} + 2\mathrm{L} \overset{K_{c,3}}{\rightleftharpoons} \mathrm{ZrCl_3(OR)L_2} \quad (13)$$

$$\mathrm{ZrCl_3(OR)L_2} + \mathrm{ZrCl_3(OR)} \overset{K_{d,3}}{\rightleftharpoons} \mathrm{ZrCl_4L_2} + \mathrm{ZrCl_2(OR)_2} \quad (14)$$

$$\mathrm{ZrCl_4L_2} \overset{K_{cc,4}}{\rightleftharpoons} \mathrm{ZrCl_4L} + \mathrm{L} \quad (15)$$

For the Job plots of ZrCl$_2$(O^{i}Pr)$_2$ and of ZrCl(O^{i}Pr)$_3$ we used a different set of reactions. Eqn (16) and (19) represent the complexation of the respective alkoxy chloride complex with TOPO. This is complemented by two disproportionations eqn (17) and (18) for ZrCl$_2$(O^{i}Pr)$_2$, and eqn (20) and (21) for ZrCl(O^{i}Pr)$_3$. The second disproportionation equation has been added in each case since the NMR spectrum of ZrCl$_2$(O^{i}Pr)$_2$ features the presence of ZrCl$_3$(O^{i}Pr)(TOPO)$_2$ and ZrCl$_4$(TOPO)$_2$ when TOPO is added. Similar observations are made for ZrCl(O^{i}Pr)$_3$.

$$\mathrm{ZrCl_2(OR)_2} + 2\mathrm{L} \overset{K_{c,2}}{\rightleftharpoons} \mathrm{ZrCl_2(OR)_2L_2} \quad (16)$$

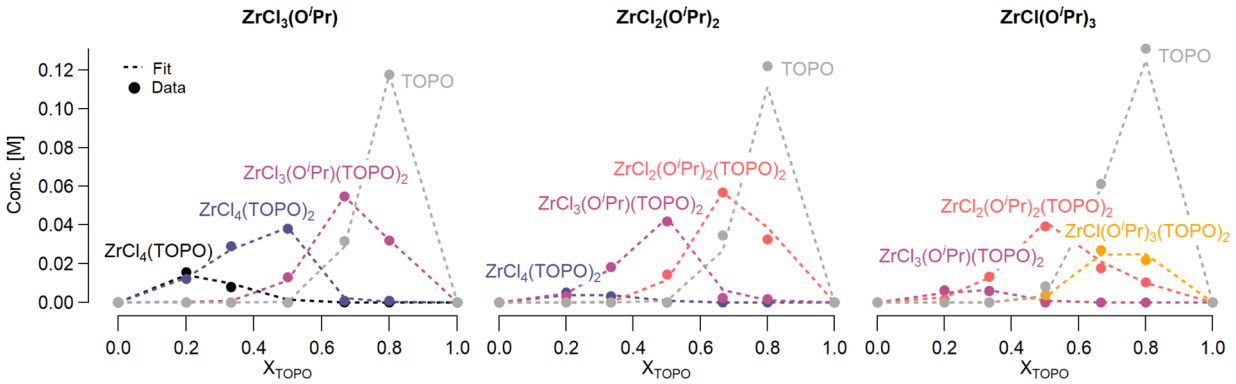

Fig. 3 Job plots of $ZrCl_3(O^iPr)$, $ZrCl_2(O^iPr)_2$ and $ZrCl(O^iPr)_3$. The dots represent the data and the dashed lines the quantitative fit. Various species formed during the reaction are indicated and plotted against the mole fraction of TOPO (X_{TOPO}). The concentration of each species was calculated by integrating the corresponding peak from the ^{31}P NMR, see ESI.†

$$ZrCl_2(OR)_2L_2 + ZrCl_2(OR)_2 \overset{K_{d,2}}{\rightleftharpoons} ZrCl_3(OR)L_2 + ZrCl(OR)_3 \quad (17)$$

$$ZrCl_3(OR)L_2 + ZrCl_2(OR)_2 \overset{K_{dd,2}}{\rightleftharpoons} ZrCl_4L_2 + ZrCl(OR)_3 \quad (18)$$

$$ZrCl(OR)_3 + 2L \overset{K_{c,3}}{\rightleftharpoons} ZrCl(OR)_3L_2 \quad (19)$$

$$ZrCl(OR)_3L_2 + ZrCl(OR)_3 \overset{K_{d,3}}{\rightleftharpoons} ZrCl_2(OR)_2L_2 + Zr(OR)_4 \quad (20)$$

$$ZrCl_2(OR)_2L_2 + ZrCl(OR)_3 \overset{K_{dd,3}}{\rightleftharpoons} ZrCl_3(OR)L_2 + Zr(OR)_4 \quad (21)$$

For all three cases, we obtain excellent fits to the data (Fig. 3 and details in the ESI†). The equilibrium constants are reported in Table 2. The complexation constant ($K_{c,x}$) decreases with decreasing chloride content but the trend is not linear. $K_{c,x}$ is slightly higher for $ZrCl_3(O^iPr)$ than for $ZrCl_2(O^iPr)_2$, but drops two orders of magnitude for $ZrCl(O^iPr)_3$, which might be due to steric effects of the isopropoxides in addition to a decreasing Lewis acidity. The opposite trend is found for the disproportionation constant ($K_{d,x}$), which is statistically the same for $ZrCl_3(O^iPr)$ and $ZrCl_2(O^iPr)_2$ but increases for $ZrCl(O^iPr)_3$. This is likely due to the larger difference in complexation strength between $ZrCl_2(O^iPr)_2$ and $ZrCl(O^iPr)_3$ compared to the difference between $ZrCl_3(O^iPr)$ and $ZrCl_2(O^iPr)_2$.

Table 2 Equilibrium constants for the sets of equilibrium reactions that describe the complexation and disproportionation mechanisms of the three zirconium alkoxy chloride complexes

	$ZrCl_3(O^iPr)$	$ZrCl_2(O^iPr)_2$	$ZrCl(O^iPr)_3$
$K_{c,x}$	$9.1 \times 10^6 \pm 6.9 \times 10^6$	$1.6 \times 10^6 \pm 1.3 \times 10^6$	$4.6 \times 10^4 \pm 2.6 \times 10^4$
$K_{cc,4}$	$1.3 \times 10^{-5} \pm 0.6 \times 10^{-5}$		
$K_{d,x}$	13.9 ± 3.2	14.5 ± 5.8	116.9 ± 63.5
$K_{dd,x}$		0.07 ± 0.01	0.16 ± 0.02

2.4. Computational insights

We sought to compare our experimental data with computations and further strengthen our hypothesis for the disproportionation driving force. Following our earlier established method based on DFT (see Experimental section), we optimized the structures of $ZrCl_x(O^iPr)_{4-x}$ (x = 1–4) and their complexes with THF or with triethylphosphine oxide (TEPO). TEPO is computationally less demanding than TOPO and forms identical complexes, as shown in Fig. S11.† All optimized structures are available as structure files in the ESI.† We considered all isomers for both THF and TEPO complexes, optimized their geometry, and calculated their energy, see Fig. 4 for TEPO (and Fig. S12† for THF). For all THF complexes, we find that the lowest energy isomer has the THF ligands in the *cis* configuration, consistent with the single-crystal data of $ZrCl_4(THF)_2$. The TEPO complexes show surprising trends. The $ZrCl_3(O^iPr)(TEPO)_2$ complex is most stable in the TEPO-*trans* configuration (Fig. 4), again consistent with the single-crystal data of $ZrCl_4(TPPO)_2$. However, the $ZrCl_2(O^iPr)_2(TEPO)_2$ complex prefers the Cl-*trans* isomer, with the TEPO ligands *cis* to each other. This configuration is most effective in reducing the steric interactions between isopropoxides and TEPO ligands. It is interesting to examine the structure of the Cl-*trans* isomer. The octahedral coordination is distorted, with the Cl–Zr–Cl bond angle measuring 166 degrees and the chloride atoms pushed towards the TEPO side. The alpha carbon of the isopropoxide ligands (*i.e.*, the branching point or the origin of sterical hindrance) is located at 3.19 and 3.34 Å from the central Zr atom. This makes isopropoxide a more steric ligand than TEPO since the Zr–P distance is longer: 3.50 and 3.68 Å (for TEPO, phosphorus is the branching point). The $ZrCl(O^iPr)_3(TEPO)_2$ complex prefers the OR-fac isomer (Fig. 4), again with the TEPO ligands in the *cis* configuration, and the octahedral coordination distorted with chloride being pushing towards TEPO. The TEPO-*trans* isomer is only 7 kJ mol^{-1} less stable though.

Using the calculated energies, we computed the enthalpy changes for the (gas-phase) complexation reactions (Table 3),

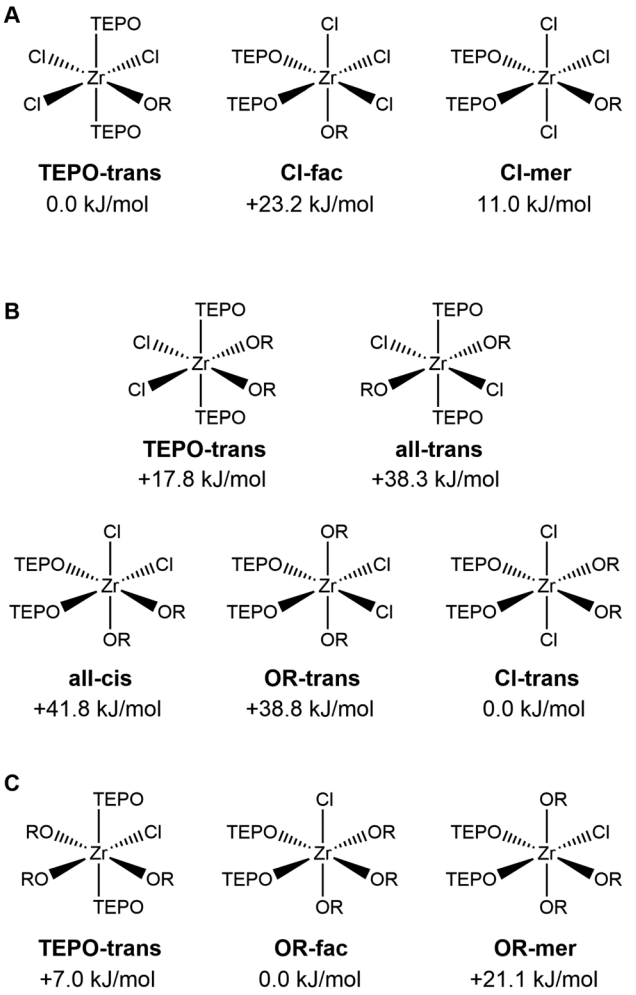

Fig. 4 The different possible isomers for the $ZrCl_x(O^iPr)_{4-x}(TEPO)_2$ complexes (x = 1–3). The relative energy compared to the most stable isomer is indicated.

which represent the global Lewis acidity since the latter is defined as the thermodynamic tendency to form Lewis acid–base pairs.[55] All reactions are exothermic and the complexation with TEPO is favored over complexation with THF, in agreement with experimental results. The complexation reaction becomes less exothermic in the series: $ZrCl_4$ > $ZrCl_3(O^iPr)$ > $ZrCl_2(O^iPr)_2$ > $ZrCl(O^iPr)_3$. This trend in global Lewis acidity agrees with the trend in effective Lewis acidity, given by the ^{31}P NMR shifts. The calculated values of ΔH cannot be directly compared to the experimental equilibrium constants since the latter depend on ΔG. For example, for $ZrCl_3(O^iPr)$, the experimental equilibrium constant translates in $\Delta G = -39.7$ kJ mol^{-1}. The large theoretical value of ΔH is thus likely offset by an unfavorable change in entropy, as one would expect for an association equilibrium. Furthermore, the uncoordinated Lewis acid is a tetrahedral monomer in the calculations, and thus dimerization (or polymerization in case of $ZrCl_4$) may account for discrepancies with experimental results.[55] As a final disclaimer, the calculations were performed in the gas phase and no solvent effects were taken into account.

When comparing the experimental data of $ZrCl_2(O^iPr)_2(TEPO)_2$ and the theoretical calculations, we are faced with a discrepancy. Two peaks are observed in the ^{31}P NMR spectrum and we previously assigned them to the TEPO-*trans* and the all-*trans* isomers, without considering the other isomers.[11] From our current calculations, Cl-*trans* isomer is clearly preferred. This is not an effect of the chain length since the two peaks appear in the same ratio for both TEPO and TOPO. The two signals always behave as one and we did not observe one without the other. We discarded the hypothesis that the two resonances represent the two phosphine oxide ligands in the same complex since the integrals are not 1 : 1 but 0.35 : 0.65. Our current best hypothesis is that the TEPO-*trans* structure is more favorable than we currently predict by DFT. The existence of multiple isomers in solution could also explain the occurrence of many more resonances in deuteroform compared to benzene (for a given composition and stoichiometry).[11] It also points to the importance of the solvent in stabilizing certain isomers.

While acknowledging the above limitations, we computed ΔH for the spontaneous disproportionation reaction and for the Lewis base-induced disproportionation, see Table 4. The disproportionation in the absence of Lewis bases is quite endothermic (entries 1 and 2). However, when we compute ΔH for the TEPO-assisted disproportionation, the reactions become more favorable (entries 3 and 4). These calculations correspond to eqn (17) and (20) and the experimental equilibrium constants were reported in Table 2. When calculating ΔG from $K_{d,3}$, we obtain −6.5 kJ mol^{-1}, significantly smaller than the computed enthalpy change (−29 kJ mol^{-1}). We attribute this to the presence of weak Lewis bases in the reaction mixture. Indeed, it is known that esters produced during the synthesis of the mixed alkoxy chlorides can coordinate to the metal center (see eqn (7)). The effect of the presence of a weaker Lewis base (*e.g.*, THF), can be also theoretically computed, see entries 5 and 6 in Table 4. It is clear that the driving force for disproportionation decreases when THF is available to coordinate the Lewis acid sites which are not coordinated by phosphine oxide. This is reproduced experimentally for $ZrCl_3(O^iPr)$, see Fig. S13.†

Table 3 Calculated changes in enthalpy for the complexation reaction of the different zirconium isopropoxy chlorides with either tetrahydrofuran (THF) and triethylphosphine oxide (TEPO). The lowest energy isomer was used for the calculation

	ΔH (kJ mol^{-1})	
	L = THF	L = TEPO
$ZrCl_4 + 2L \rightleftharpoons ZrCl_4L_2$	−117.1	−235.0
$ZrCl_3(O^iPr) + 2L \rightleftharpoons ZrCl_3(O^iPr)L_2$	−105.3	−188.0
$ZrCl_2(O^iPr)_2 + 2L \rightleftharpoons ZrCl_2(O^iPr)_2L_2$	−90.3	−177.4
$ZrCl(O^iPr)_3 + 2L \rightleftharpoons ZrCl(O^iPr)_3L_2$	−65.3	−113.6

Table 4 Calculated changes in enthalpy for the disproportionation reaction of the different zirconium isopropoxy chlorides with L = TEPO. The lowest energy isomer was used for the calculation

Entry	Equilibrium	ΔH (kJ mol^{-1})
1	$2ZrCl_3(O^iPr) \rightleftharpoons ZrCl_4 + ZrCl_2(O^iPr)_2$	18.0
2	$2ZrCl_2(O^iPr)_2 \rightleftharpoons ZrCl_3(O^iPr) + ZrCl(O^iPr)_3$	16.9
3	$ZrCl_3(O^iPr)L_2 + ZrCl_3(O^iPr) \rightleftharpoons ZrCl_4L_2 + ZrCl_2(O^iPr)_2$	−29.0
4	$ZrCl_2(O^iPr)_2L_2 + ZrCl_2(O^iPr)_2 \rightleftharpoons ZrCl_3(O^iPr)L_2 + ZrCl(O^iPr)_3$	6.3
5	$ZrCl_3(O^iPr)L_2 + ZrCl_3(O^iPr)(THF)_2 \rightleftharpoons ZrCl_4L_2 + ZrCl_2(O^iPr)_2(THF)_2$	−13.9
6	$ZrCl_2(O^iPr)_2L_2 + ZrCl_2(O^iPr)_2(THF)_2 \rightleftharpoons ZrCl_3(O^iPr)L_2 + ZrCl(O^iPr)_3(THF)_2$	31.2

2.5. Generalization

To test the generality of the disproportionation behavior, we also investigated other alkoxy halides, varying the metal, the alkoxide and the halide. Fig. S14–S17† show the NMR spectra with 2 or 4 equivalents TOPO, to identify the complexation products. Fig. 5 shows the spectra with one equivalent of TOPO and in all four cases, the disproportionation products are detected. We observe some interesting differences. In case of zirconium isopropoxy tribromide, we notice a stronger tendency for disproportionation compared to the above zirconium isopropoxy trichloride in the presence of THF (Fig. S13†). We synthesized the alkoxy bromide by mixing $ZrBr_4(THF)_2$ and $Zr(O^iPr)_4(^iPrOH)$ due to the low solubility of $ZrBr_4$. In case of zirconium *tert*-butoxy trichloride (synthesized from $ZrCl_4(THF)_2$ and $Zr(O^tBu)_4$) we observe a stronger disproportionation compared to zirconium isopropoxy trichloride, but weaker than zirconium isopropoxy tribromide. The hafnium isopropoxy chlorides are synthesized from $HfCl_4$ and $Hf(O^iPr)_4(^iPrOH)$ so there is no THF or ester present, only 0.25 equivalents of isopropanol. A complete disproportionation is the result. In case of titanium, we observe the expected disproportionation products for $TiCl_3(O^iPr)$ and $TiCl_2(O^iPr)_2$, but not for $TiCl(O^iPr)_3$. As demonstrated in Fig. S17,† $TiCl_4(TOPO)_2$ and $TiCl_3(O^iPr)(TOPO)_2$ are detectable species with narrow resonances in the ^{31}P NMR spectrum, but $TiCl_2(O^iPr)_2(TOPO)_2$

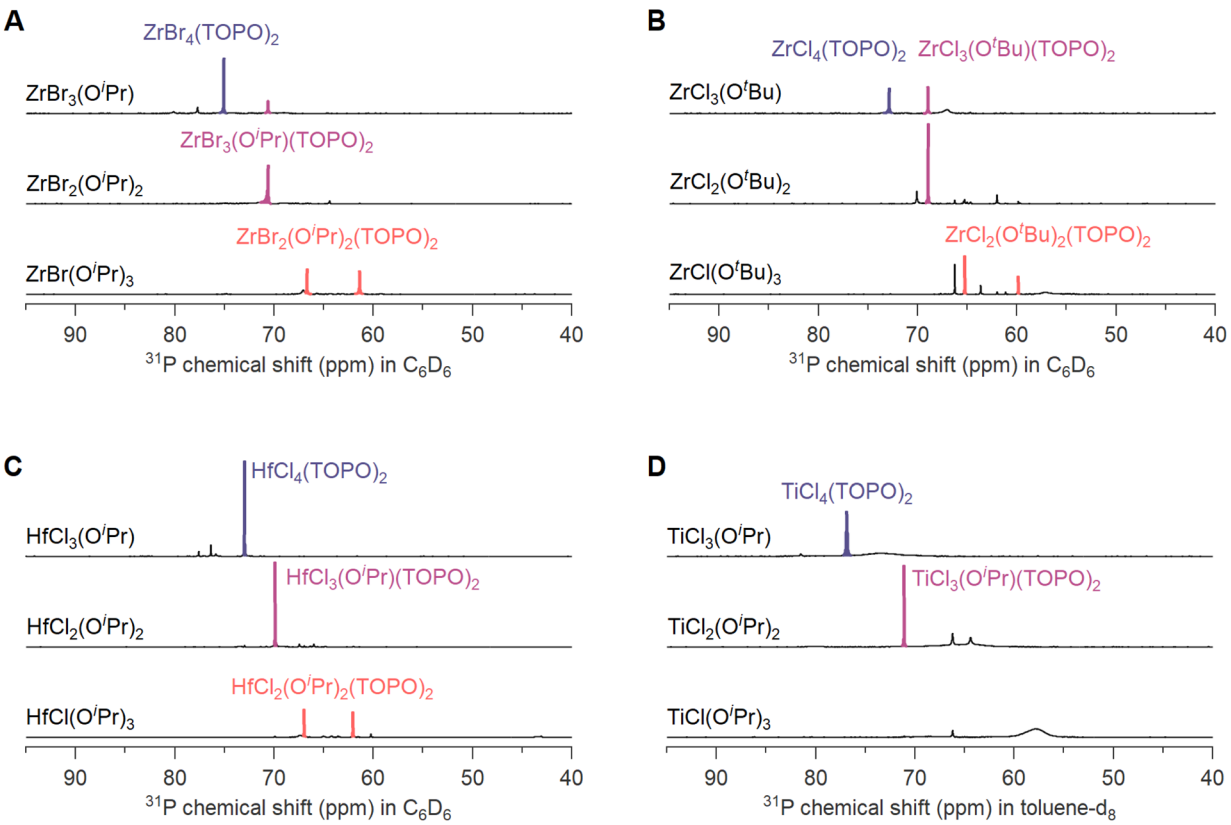

Fig. 5 ^{31}P NMR spectra of (A) zirconium isopropoxy bromide (B) zirconium *tert*-butoxy chloride (C) hafnium isopropoxy chloride (D) titanium isopropoxy chloride complexes mixed with 1 equivalent of TOPO. In case of A and B, the alkoxy halides were synthesized from the respective zirconium halide THF complex.

is not detectable, featuring very broad lines, indicative of chemical exchange between bound and free TOPO.

3. Conclusions

We studied the interaction of group 4 metal halides and metal alkoxy halides with Lewis bases. We found that phosphine oxides are excellent hard bases for these types of Lewis acids and form Lewis acid–base adducts with a 1 : 2 stoichiometry. Sub-stoichiometric amounts of Lewis bases lead to disproportionation of the metal alkoxy halides. We were able to extract the experimental equilibrium constants for both complexation and disproportionation equilibria from the Job plot. The complexation equilibrium constant decreases with the Lewis acidity of the complex, *i.e.* with the chloride content. Calculations at the DFT level of theory confirmed the trend and allowed us to rationalize the driving force for disproportionation: the formation of more stable Lewis acid–base adducts. These results thus provide fundamental insight into metal alkoxy halide Lewis acids and are also relevant for group 13 Lewis acids. The results are of direct relevance to nanocrystal reactions with TOPO as a coordinating solvent.

4. Experimental

4.1. Materials

$ZrCl_4$ (99.9%), $HfCl_4$ (99.9%), $Ti(O^iPr)_4$ (98%) and $Zr(O^tBu)_4$ (99.99%) were purchased from Strem Chemicals. $TiCl_4$ (99.99%) was bought from ACROS Organics. Acetyl chloride (≥99.0%) was provided by Sigma Aldrich. $ZrCl_4(THF)_2$, $TiCl_4(THF)_2$ and $HfCl_4(THF)_2$ were synthesized following the procedure reported by Manzer *et al.*[56] $ZrBr_4(THF)_2$ was synthesized in an identical fashion to $ZrCl_4(THF)_2$ (yield = 20%). $Zr(O^iPr)_4{\cdot}^iPrOH$ and $Hf(O^iPr)_4{\cdot}^iPrOH$ were synthesized following the procedure reported firstly by Bradley *et al.*[57] and slightly modified by Dhaene *et al.*[58] Tri-*n*-octylphosphine oxide (Strem Chemicals, 99%) was recrystallized according to the procedure described by Owen *et al.*[59] while triphenylphosphine oxide (Sigma Aldrich, 98%) was used without further purification. In benzene-d_6 (Apollo scientific, 99.5 atom%), toluene-d_8 (VWR, >99.5 atom%), chloroform-d (Eurisotop, 99.5 atom%) and anhydrous pentane (Sigma Aldrich, ≥99%) 10 vol% of activated 4 Å molecular sieves were added and left to stand for 3 days in the glovebox to remove residual water. Toluene and DCM were dried over a solvent system before being transferred into a glovebox. All operations were performed air-free in a nitrogen-filled glovebox.

4.2. Methods

Preparation of the NMR samples for the spectra in Fig. 2 and 3. $ZrCl_3(O^iPr)$, $ZrCl_2(O^iPr)_2$ and $ZrCl(O^iPr)_3$ were synthesized according to the procedure reported by Bradley *et al.*,[42] by mixing $Zr(O^iPr)_4$ and acetyl chloride in different molar ratios. After stirring for 48 hours at room temperature, the solvent is removed and three 0.5 M solutions were prepared in C_6D_6 (1 mmol of $ZrCl_x(O^iPr)_{4-x}$ in 2 mL C_6D_6), together with various volumes of a 0.5 M solution of TOPO (773.3 mg, 2 mmol) in C_6D_6 (3.12 mL). The different NMR tubes were prepared according to Table 5.

The ^1H NMR and ^{31}P NMR spectra are shown in Fig. S8–S10.† All the peaks in the ^{31}P NMR spectra were integrated and their sum was normalized for the total amount of TOPO in the solution. For the complexes with two TOPO ligands, the concentration of the complex is half of the bound TOPO concentration. The detailed procedure to obtain the Job Plot is provided in the ESI.†

Preparation of the NMR samples for the spectra in Fig. 5. $ZrBr_x(O^iPr)_{4-x}$ complexes were synthesized by mixing $ZrBr_4(THF)_2$ with $Zr(O^iPr)_4$ in the right molar ratios and dissolved in C_6D_6 to obtain three 0.1 M stock solutions. The NMR tubes are prepared by mixing the 0.1 M C_6D_6 solution of $ZrBr_x(O^iPr)_{4-x}$ (200 μL) with a 0.5 M C_6D_6 solution of TOPO (40 μL for 1 equivalent, 80 μL for 2 equivalents) and C_6D_6 is added to make up the tubes to a total volume of 400 μL.

$ZrCl_x(O^tBu)_{4-x}$ complexes were synthesized by mixing $ZrCl_4(THF)_2$ with $Zr(O^tBu)_4$ in the right molar ratios and dissolved in C_6D_6 to obtain three 0.5 M stock solutions (0.5 mmol $ZrCl_x(O^tBu)_{4-x}$ in 1 mL C_6D_6). To improve the solubility of the complexes, 1 equivalent of TOPO is added in each of the three stock solutions (1 mL of 0.5 M C_6D_6 solution of TOPO). The NMR tubes for 1 equivalent are prepared by diluting the solution of $ZrCl_x(O^tBu)_{4-x}$ with 1 equiv. TOPO (100 μL) with C_6D_6 (400 μL). To prepare the NMR tubes with 4 equiv., the solution of $ZrCl_x(O^tBu)_{4-x}$ with 1 equiv. TOPO (100 μL) is mixed with 0.5 M C_6D_6 of TOPO (150 μL) and C_6D_6 (250 μL).

$HfCl_x(O^iPr)_{4-x}$ complexes were synthesized by mixing $HfCl_4$ with $Hf(O^iPr)_4$ in the right molar ratios and dissolved in C_6D_6 to obtain three 0.5 M stock solutions (0.5 mmol $HfCl_x(O^iPr)_{4-x}$ in 1 mL C_6D_6). To improve the solubility of the complexes, 1 equivalent of TOPO is added in each of the three stock solutions (1 mL of 0.5 M C_6D_6 solution of TOPO). The NMR tubes for 1 equivalent are prepared by diluting the solution of $HfCl_x(O^iPr)_{4-x}$ with 1 equiv. TOPO (100 μL) with C_6D_6 (400 μL). To prepare the NMR tubes with 4 equiv., the solution of $HfCl_x(O^iPr)_{4-x}$ with 1 equiv. TOPO (100 μL) is mixed with 0.5 M C_6D_6 of TOPO (150 μL) and C_6D_6 (250 μL).

$TiCl_x(O^iPr)_{4-x}$ complexes were synthesized by mixing 0.5 M C_6D_6 solution of $TiCl_4$ with a 0.5 M C_6D_6 solution of $Ti(O^iPr)_4$ in the right volumes. The NMR tubes are prepared by mixing the

Table 5 Details of the preparation of the NMR tubes. For each $ZrCl_x(O^iPr)_{4-x}$ the 5 NMR have been prepared

X_{TOPO}	$n_{ZrCl_x(O^iPr)_{4-x}}$ (mmol)	n_{TOPO} (mmol)	$V_{ZrCl_x(O^iPr)_{4-x}}$ (μL)	V_{TOPO} (μL)	$V_{C_6D_6}$ (μL)
0.2	0.12	0.03	240	60	300
0.33	0.1	0.05	200	100	300
0.5	0.075	0.075	150	150	300
0.66	0.05	0.1	100	200	300
0.8	0.03	0.12	60	240	300

0.5 M C_6D_6 solution of $TiCl_x(O^iPr)_{4-x}$ (150 μL for 1 equiv. TOPO, 60 μL for 4 equiv. TOPO) with a 0.5 M C_6D_6 solution of TOPO (150 μL for 1 equivalent, 240 μL for 4 equivalents) and C_6D_6 is added to make up the tubes to a total volume of 500 μL.

Crystal growth of $ZrCl_4(TPPO)_2$. 1.5 mL of a 0.1 M toluene solution of TPPO (69.6 mg, 0.25 mmol TPPO in 2.5 mL of toluene) was layered over a 0.1 M DCM solution of $ZrCl_4(THF)_2$ (37.7 mg, 0.1 mmol $ZrCl_4(THF)_2$ in 1 mL of DCM) in a 4 mL vial. White crystals grew after 4 days and a single crystal was chosen for X-ray diffraction, while the rest was dried under vacuum and analyzed by PXRD and ^{31}P NMR. Yield of 44%. A detailed characterization consisting of ^1H NMR and ^{31}P NMR (Fig. S2), PXRD (Fig. S4), IR (Fig. S3) and TGA (Table S3) is reported in the ESI.†

Crystal growth of $HfCl_4(TPPO)_2$. 1.5 mL of a 0.1 M toluene solution of TPPO (69.6 mg, 0.25 mmol TPPO in 2.5 mL of toluene) was layered over a 0.1 M DCM solution of $HfCl_4(THF)_2$ (46.5 mg, 0.1 mmol $HfCl_4(THF)_2$ in 1 mL of DCM) in a 4 mL vial. White crystals grew after 4 days and a single crystal was chosen for X-ray diffraction, while the rest was dried under vacuum and analyzed by PXRD and ^{31}P NMR. Yield of 38%. A detailed characterization consisting of ^1H NMR and ^{31}P NMR (Fig. S2), PXRD (Fig. S4), IR (Fig. S3) and TGA (Table S3) is reported in the ESI.†

Crystal growth of $TiCl_4(TPPO)_2$. Anhydrous toluene (0.5 mL) was layered over a 0.1 M DCM solution of $TiCl_4(THF)_2$ (33.3 mg, 0.1 mmol $TiCl_4(THF)_2$ in 1 mL DCM) in a 4 mL vial. On top of it, 1 mL of a 0.05 M toluene solution of TPPO (69.6 mg, 0.25 mmol TPPO in 5 mL of toluene) was layered. Yellow crystals grew after 20 hours and a single crystal was chosen for X-ray diffraction, while the rest was dried under vacuum and analyzed by PXRD and ^{31}P NMR. Yield of 74%. A detailed characterization consisting of ^1H NMR and ^{31}P NMR (Fig. S2), PXRD (Fig. S4), IR (Fig. S3) and TGA (Table S3) is reported in the ESI.†

Crystal growth of $ZrBr_4(TPPO)_2$. $ZrBr_4$ (4.1 mg, 0.01 mmol) is dissolved in anhydrous DCM (2 mL) and TPPO (7.0 mg, 0.025 mmol) is added to the solution. Anhydrous pentane (2 mL) was layered over it. A single crystal was selected for X-ray diffraction. Quantitative yield. A detailed characterization consisting of ^1H NMR and ^{31}P NMR (Fig. S2), PXRD (Fig. S4), IR (Fig. S3) and TGA (Table S3) is reported in the ESI.†

Crystal growth of $ZrBr_4(THF)_2$ by recrystallization. $ZrBr_4(THF)_2$ is dissolved in anhydrous DCM, and filtrated to remove $ZrBr_4$ impurities. $ZrBr_4(THF)_2$ is then precipitated from the solution with anhydrous pentane, vacuum dried and again dissolved in anhydrous DCM. White crystals grew after 2 days through diffusing pentane vapor. A single crystal was selected for X-ray diffraction. A detailed characterization consisting of ^1H NMR and ^{31}P NMR (Fig. S2), PXRD (Fig. S4), IR (Fig. S3) and TGA (Table S3) is reported in the ESI.†

4.3. General instrumentation

Nuclear magnetic resonance (NMR) measurements were recorded at 298 K on Bruker UltraShield 500 spectrometer operating at a frequency of 500.13 MHz. Regular ^1H, and ^{31}P NMR spectra were acquired using the standard pulse sequences with a 30 degree pulse with a recycle delay of 1.5, and 1.0 second from the Bruker library; zg30, zgpg30 respectively. ^{31}P NMR spectra were acquired using inverse gated decoupling and 64 scans and were processed with a line broadening of 5 Hz. All resonances are background-corrected. Chemical shifts (δ) are given in parts per million (ppm), and the residual solvent peak was used as an internal standard (C_6D_6: δH = 7.16 ppm, $CDCl_3$: δH = 7.26 ppm, tol-d_8: δH = 2.09 ppm).

Single crystal XRD. Single crystal data were collected on STOE STADIVARI diffractometer with a microfocused Cu source. The crystals were kept at a steady T = 150 K during data collection. The structures were solved with the ShelXT[60] solution program using dual methods and by using Olex2[61] as the graphical interface. The model was refined with ShelXL 2018/3[62] using full matrix least squares minimization on F^2.

Quantum chemical calculations. All calculations were performed with the B3LYP functional together with the aug-cc-pVDZ basis set for C, H, O, Cl, and P atoms using Gaussian09.[63–66] The aug-cc-pVDZ pseudopotential and associated basis set of Peterson *et al.* was taken from the Basis Set Exchange and applied to the Zr atoms.[67,68] This level of theory was previously shown to be accurate for these types of metal complexes.[11] Only calculations in the gas phase were carried out. To calculate the ^{31}P NMR chemical shifts from the optimized structures, we followed the protocol of Willoughby *et al.*[69]

Powder X-ray diffraction (PXRD). PXRD patterns were collected at room temperature in transmission mode using a Stoe Stadi P diffractometer with a micro-focused Cu-Kα-source (λ = 1.542 Å) equipped with a DECTRIS MYTHEN 1K detector.

Fourier transform infrared spectroscopy (FTIR). FTIR spectra were recorded air-free in a nitrogen-filled glovebox in transmission mode on a Bruker Alpha II FTIR-Spectrometer. The measured pellets were prepared air-free by mixing the sample with potassium bromide and compressing them.

Thermogravimetric analysis (TGA). TGA was performed on a TGA5500 (TA instruments) instrument. The samples were heated to 800 °C at a ramping rate of 5 °C min^{-1}. At the end an isotherm of 15 min is given to ensure that all the organics are burned out.

Conflicts of interest

There are no conflicts to declare.

Acknowledgements

The authors thank the SNSF Eccelenza funding scheme (project number: 194172) and the Swiss Nanoscience Institute for funding. The authors thank Prof. Daniel Häussinger for fruitful discussions and scientific assistance regarding NMR spectroscopy. The authors thank Dr Sven Sahle and Dr Frank

Bergmann for their support in operating the modeling program COPASI. The authors thank Prof. Markus Meuwly and Dr Mike Devereux for setting up the computational calculations and fruitful discussions. The authors acknowledge Jikson Pulparayil Mathew for helping with TGA measurements, Prof. Murielle F. Delley for providing the air-free IR instrumentation setup, and Vanessa Wyss for helping with the IR measurements.

References

1 N. N. Greenwood and A. Earnshaw, in *Titanium, Zirconium and Hafnium*, Elsevier, 1997, book section 21, pp. 954–975.
2 P. Arnal, R. J. P. Corriu, D. Leclercq, P. H. Mutin and A. Vioux, A Solution Chemistry Study of Nonhydrolytic Sol-Gel Routes to Titania, *Chem. Mater.*, 1997, **9**, 694–698.
3 A. Vioux, Nonhydrolytic Sol-Gel Routes to Oxides, *Chem. Mater.*, 1997, **9**, 2292–2299.
4 T. J. Trentler, T. E. Denler, J. F. Bertone, A. Agrawal and V. L. Colvin, Synthesis of TiO_2 Nanocrystals by Nonhydrolytic Solution-Based Reactions, *J. Am. Chem. Soc.*, 1999, **121**, 1613–1614.
5 M. Niederberger, M. H. Bartl and G. D. Stucky, Benzyl alcohol and titanium tetrachloride - A versatile reaction system for the nonaqueous and low-temperature preparation of crystalline and luminescent titania nanoparticles, *Chem. Mater.*, 2002, **14**, 4364–4370.
6 M. Niederberger and G. Garnweitner, Organic Reaction Pathways in the Nonaqueous Synthesis of Metal Oxide Nanoparticles, *Chemistry*, 2006, **12**, 7282–7302.
7 D. Van den Eynden, R. Pokratath and J. De Roo, Nonaqueous Chemistry of Group 4 Oxo Clusters and Colloidal Metal Oxide Nanocrystals, *Chem. Rev.*, 2022, **122**, 10538–10572.
8 M. Parvizian and J. De Roo, Precursor chemistry of metal nitride nanocrystals, *Nanoscale*, 2021, **13**, 18865–18882.
9 R. Deshmukh and M. Niederberger, Mechanistic Aspects in the Formation, Growth and Surface Functionalization of Metal Oxide Nanoparticles in Organic Solvents, *Chem. – Eur. J.*, 2017, **23**, 8542–8570.
10 C. Suchomski, D. Weber, P. Dolcet, A. Hofmann, P. Voepel, J. Yue, M. Einert, M. Möller, S. Werner, S. Gross, *et al.*, Sustainable and surfactant-free high-throughput synthesis of highly dispersible zirconia nanocrystals, *J. Mater. Chem. A*, 2017, **5**, 16296–16306.
11 R. Pokratath, D. Van den Eynden, S. R. Cooper, J. K. Mathiesen, V. Waser, M. Devereux, S. J. L. Billinge, M. Meuwly, K. M. O. Jensen and J. De Roo, Mechanistic Insight into the Precursor Chemistry of ZrO_2 and HfO_2 Nanocrystals; towards Size-Tunable Syntheses, *JACS Au*, 2022, **2**, 827–838.
12 J. Joo, T. Yu, Y. W. Kim, H. M. Park, F. Wu, J. Z. Zhang and T. Hyeon, Multigram Scale Synthesis and Characterization of Monodisperse Tetragonal Zirconia Nanocrystals, *J. Am. Chem. Soc.*, 2003, **125**, 6553–6557.
13 R. Pokratath, L. Lermusiaux, S. Checchia, J. P. Mathew, S. R. Cooper, J. K. Mathiesen, G. Landaburu, S. Banerjee, S. Tao, N. Reichholf and J. De Roo, An Amorphous Phase Precedes Crystallization: Unraveling the Colloidal Synthesis of Zirconium Oxide Nanocrystals, *ACS Nano*, 2023, **17**, 8796–8806.
14 J. Tang, J. Fabbri, R. D. Robinson, Y. Zhu, I. P. Herman, M. L. Steigerwald and L. E. Brus, Solid-Solution Nanoparticles: Use of a Nonhydrolytic Sol-Gel Synthesis To Prepare HfO_2 and $Hf_xZr_{1-x}O_2$ Nanocrystals, *Chem. Mater.*, 2004, **16**, 1336–1342.
15 S. W. Depner, K. R. Kort and S. Banerjee, Precursor control of crystal structure and stoichiometry in twin metal oxide nanocrystals, *CrystEngComm*, 2009, **11**, 841–846.
16 S. W. Depner, N. D. Cultrara, K. E. Farley, Y. Qin and S. Banerjee, Ferroelastic Domain Organization and Precursor Control of Size in Solution-Grown Hafnium Dioxide Nanorods, *ACS Nano*, 2014, **8**, 4678–4688.
17 G. R. Waetzig, S. W. Depner, H. Asayesh-Ardakani, N. D. Cultrara, R. Shahbazian-Yassar and S. Banerjee, Stabilizing metastable tetragonal HfO_2 using a non-hydrolytic solution-phase route: ligand exchange as a means of controlling particle size, *Chem. Sci.*, 2016, **7**, 4930–4939.
18 T. Ohlerth, H. Du, T. Hammoor, J. Mayer and U. Simon, Tailoring of Colloidal HfO_2 Nanocrystals with Unique Morphologies and New Self-Assembly Features, *Small Sci.*, 2024, 2300209.
19 R. L. Davidovich, D. V. Marinin, V. Stavila and K. H. Whitmire, Structural chemistry of fluoride and oxofluoride complexes of titanium(IV), *Coord. Chem. Rev.*, 2015, **299**, 61–82.
20 B. Krebs, Die Kristallstruktur von Zirkoniumtetrachlorid, *Z. Anorg. Allg. Chem.*, 1970, **378**, 263–272.
21 H. Bialowons, M. Müller and B. G. Müller, Titantetrafluorid – Eine überraschend einfache Kolumnarstruktur, *Z. Anorg. Allg. Chem.*, 1995, **621**, 1227–1231.
22 G. B. Nikiforov, H. W. Roesky and D. Koley, A survey of titanium fluoride complexes, their preparation, reactivity, and applications, *Coord. Chem. Rev.*, 2014, **258–259**, 16–57.
23 D. S. Dyer and R. O. Ragsdale, Fluorine-19 nuclear magnetic resonance study of some titanium tetrafluoride-substituted pyridine 1-oxide adducts, *Inorg. Chem.*, 1969, **8**, 1116–1120.
24 M. Jura, W. Levason, E. Petts, G. Reid, M. Webster and W. Zhang, Taking TiF_4 complexes to extremes-the first examples with phosphine co-ligands, *Dalton Trans.*, 2010, **39**, 10264–10271.
25 M. Nieger, L. Szarvas and D. Gudat, *CSD Communication*, 2022.
26 F. Calderazzo, U. Englert, G. Pampaloni and M. Volpe, Redox reactions with bis (η_6-arene) derivatives of early transition metals, *J. Organomet. Chem.*, 2005, **690**, 3321–3332.
27 M. Eberle and C. Röhr, Tetrachlorobis (tetrahydrofuran-O) zirconium(IV), *Acta Crystallogr., Sect. C: Cryst. Struct. Commun.*, 1996, **52**, 566–568.

28 S. Duraj, R. Towns, R. Baker and J. Schupp, Structure of *cis*-tetrachlorobis (tetrahydrofuran) hafnium(IV), *Acta Crystallogr., Sect. C: Cryst. Struct. Commun.*, 1990, **46**, 890–892.

29 C. E. F. Rickard, M. W. Glenny and A. J. Nielson, Tetrachloro(*N*,*N*,*N*′,*N*′-tetra-methyl-ethyl-enediamine)-zirconium (IV), *Acta Crystallogr., Sect. E: Struct. Rep. Online*, 2003, **59**, m183–m184.

30 S. Troyanov, G. Mazo and M. Simonov, *Koord. Khim.*, 1985, **11**, 1147.

31 S. Rabe and U. Müller, Die Kristallstrukturen von PPh_4 $[MCl_5(NCMe)]\cdot MeCN$ (M = Ti, Zr), zwei Modifikationen von PPh_4 $[TiCl_5$ (NCMe)] und von *cis*-$TiCl_4(NCMe)_2\cdot MeCN$, *Z. Anorg. Allg. Chem.*, 2001, **627**, 201–205.

32 S. Troyanov, G. Mazo, M. Simonov and A. Il'inskii, *Zh. Neorg. Khim.*, 1986, **31**, 3022.

33 S. Troyanov, G. Mazo and M. Simonov, *Koord. Khim.*, 1986, **12**, 1000.

34 J. Guery, C. Leblanc and M. Jacoboni, *Eur. J. Solid State Inorg. Chem.*, 1989, **26**, 289.

35 S. Troyanov, G. Mazo and M. Simonov, *Vestn. Mosk. Univ., Ser. 2: Khim.*, 1986, **27**, 575.

36 S. Troyanov and M. Subbotin, *Zh. Neorg. Khim.*, 1987, **32**, 58.

37 D. S. Dyer and R. O. Ragsdale, *cis–trans*-Isomerism in titanium tetrafluoride–substituted pyridine 1-oxide adducts, *Chem. Commun.*, 1966, 601–602.

38 D. S. Dyer and R. O. Ragsdale, The Mechanism of Fluorine-19 Exchange in the $TiF_4\cdot 2$(Donor) Complexes, *J. Am. Chem. Soc.*, 1967, **89**, 1528–1529.

39 G. B. Nikiforov, C. Knapp, J. Passmore and A. Decken, Interaction of TiF_4 with the donor solvents SO_2, PhCN, and MeCN: Isolation and structural characterization of the first trimeric fluorine bridged donor–acceptor adduct $\{TiF_4$ (PhCN)$\}_3$, *J. Fluorine Chem.*, 2006, **127**, 1398–1404.

40 H. Weingarten and J. R. Van Wazer, Exchange of Parts between Molecules at Equilibrium. VI. Scrambling on Titanium of the Alkoxyl, Dimethylamino, and Halogen Substituents, *J. Am. Chem. Soc.*, 1965, **87**, 724–730.

41 D. C. Bradley, R. C. Mehrotra, I. P. Rothwell and A. Singh, *Alkoxo and Aryloxo Derivatives of Metals*, Academic Press, London, 2001.

42 D. Bradley, F. Abd-El Halim, R. Mehrotra and W. Wardlaw, 898. Reactions of acetyl chloride with zirconium alkoxides, *J. Chem. Soc.*, 1952, 4609–4612.

43 S. Hoops, S. Sahle, R. Gauges, C. Lee, J. Pahle, N. Simus, M. Singhal, L. Xu, P. Mendes and U. Kummer, COPASI: a COmplex PAthway SImulator, *Bioinformatics*, 2006, **22**, 3067–3074.

44 U. Mayer, V. Gutmann and W. Gerger, The acceptor number – A quantitative empirical parameter for the electrophilic properties of solvents, *Monatsh. Chem.*, 1975, **106**, 1235–1257.

45 M. A. Beckett, G. C. Strickland, J. R. Holland and K. Sukumar Varma, A convenient n.m.r. method for the measurement of Lewis acidity at boron centres: correlation of reaction rates of Lewis acid initiated epoxide polymerizations with Lewis acidity, *Polymer*, 1996, **37**, 4629–4631.

46 M.-F. Li and Y.-K. Shan, Crystal structure of *trans*-bis (triphenylphospine oxide) tetrachlorotitanum (IV), $TiCl_4[(C_6H_5)_3PO]_2$, *Z. Kristallogr. - New Cryst. Struct.*, 2006, **221**, 41–42.

47 S. L. Benjamin, W. Levason, D. Pugh, G. Reid and W. Zhang, Preparation and structures of coordination complexes of the very hard Lewis acids ZrF_4 and HfF_4, *Dalton Trans.*, 2012, **41**, 12548–12557.

48 D. C. Bradley, D. C. Hancock and W. Wardlaw, 524. Titanium chloride alkoxides, *J. Chem. Soc.*, 1952, 2773–2778.

49 E. Wiberg and W. Sütterlin, Zur Kenntnis einiger Verbindungen vom Typus $BCl_{3-n}(OR)_n$ 2. Mitteilung. Über Disproportionierungen in der Verbindungsreihe $BCl_{3-n}(OCH_3)_n$, *Z. Anorg. Allg. Chem.*, 1935, **222**, 92–97.

50 E. Wiberg and H. Smedsrud, Über Verbindungen des Typus $BCl_{3-n}(OR)_n$. 3. Mitteilung. Darstellung von BCl_2OCH_3 und $BCl(OCH_3)_2$ aus Borchlorid und Borsäure-methylester, *Z. Anorg. Allg. Chem.*, 1935, **225**, 204–208.

51 I. Ostromisslensky, Über eine neue, auf dem Massenwirkungsgesetz fußende Analysenmethode einiger binären Verbindungen, *Ber. Dtsch. Chem. Ges.*, 1911, **44**, 268–273.

52 R. B. Denison, Contributions to the knowledge of liquid mixtures—I. Property-composition curves and the molecular changes which take place on forming binary liquid mixtures, *Trans. Faraday Soc.*, 1912, **8**, 20–34.

53 P. Job, Formation and stability of inorganic complexes in solution, *Ann. Chim.*, 1928, **9**, 113–134.

54 E. J. Olson and P. Bühlmann, Getting more out of a Job plot: determination of reactant to product stoichiometry in cases of displacement reactions and *n:n* complex formation, *J. Org. Chem.*, 2011, **76**, 8406–8412.

55 P. Erdmann and L. Greb, What Distinguishes the Strength and the Effect of a Lewis Acid: Analysis of the Gutmann–Beckett Method, *Angew. Chem.*, 2022, **134**, e202114550.

56 L. E. Manzer, J. Deaton, P. Sharp and R. R. Schrock, in *31. Tetrahydrofuran Complexes of Selected Early Transition Metals*, 1982, vol. 21, pp. 135–140.

57 D. Bradley, R. Mehrotra and W. Wardlaw, 330. Hafnium alkoxides, *J. Chem. Soc.*, 1953, 1634–1636.

58 E. Dhaene, C. Seno and J. De Roo, Synthesis of zirconium(IV) and hafnium(IV) isopropoxide, sec-butoxide and *tert*-butoxide, *ChemRxiv*, 2023, DOI: **10.26434/chemrxiv-2023-4s67j-v2**.

59 J. S. Owen, J. Park, P.-E. Trudeau and A. P. Alivisatos, Reaction chemistry and ligand exchange at cadmium- selenide nanocrystal surfaces, *J. Am. Chem. Soc.*, 2008, **130**, 12279–12281.

60 G. M. Sheldrick, SHELXT-Integrated space-group and crystal-structure determination, *Acta Crystallogr., Sect. A: Found. Adv.*, 2015, **71**, 3–8.

61 O. V. Dolomanov, L. J. Bourhis, R. J. Gildea, J. A. Howard and H. Puschmann, OLEX2: a complete structure solution, refinement and analysis program, *J. Appl. Crystallogr.*, 2009, **42**, 339–341.

62 G. M. Sheldrick, Crystal structure refinement with SHELXL, *Acta Crystallogr., Sect. C: Struct. Chem.*, 2015, **71**, 3–8.

63 M. J. Frisch, G. W. Trucks, H. B. Schlegel, G. E. Scuseria, M. A. Robb, J. R. Cheeseman, G. Scalmani, V. Barone, B. Mennucci, G. A. Petersson, H. Nakatsuji, M. Caricato, X. Li, H. P. Hratchian, A. F. Izmaylov, J. Bloino, G. Zheng, J. L. Sonnenberg, M. Hada, M. Ehara, K. Toyota, R. Fukuda, J. Hasegawa, M. Ishida, T. Nakajima, Y. Honda, O. Kitao, H. Nakai, T. Vreven, J. A. Montgomery, J. E. Peralta, F. Ogliaro, M. Bearpark, J. J. Heyd, E. Brothers, K. N. Kudin, V. N. Staroverov, R. Kobayashi, J. Normand, K. Raghavachari, A. Rendell, J. C. Burant, S. S. Iyengar, J. Tomasi, M. Cossi, N. Rega, J. M. Millam, M. Klene, J. E. Knox, J. B. Cross, V. Bakken, C. Adamo, J. Jaramillo, R. Gomperts, R. E. Stratmann, O. Yazyev, A. J. Austin, R. Cammi, C. Pomelli, J. W. Ochterski, R. L. Martin, K. Morokuma, V. G. Zakrzewski, G. A. Voth, P. Salvador, J. J. Dannenberg, S. Dapprich, A. D. Daniels, Ö. Farkas, J. B. Foresman, J. V. Ortiz, J. Cioslowski and D. J. Fox, *Gaussian 09 Revision B.01*, Gaussian, Inc., Wallingford, 2009.

64 A. D. Becke, Density-functional exchange-energy approximation with correct asymptotic behavior, *Phys. Rev. A*, 1988, **38**, 3098–3100.

65 R. A. Kendall, T. H. Dunning and R. J. Harrison, Electron affinities of the first-row atoms revisited. Systematic basis sets and wave functions, *J. Chem. Phys.*, 1992, **96**, 6796–6806.

66 C. Lee, W. Yang and R. G. Parr, Development of the Colle-Salvetti correlation-energy formula into a functional of the electron density, *Phys. Rev. B: Condens. Matter Mater. Phys.*, 1988, **37**, 785–789.

67 K. A. Peterson, D. Figgen, M. Dolg and H. Stoll, Energy-consistent relativistic pseudopotentials and correlation consistent basis sets for the 4d elements Y–Pd, *J. Chem. Phys.*, 2007, **126**, 124101.

68 B. P. Pritchard, D. Altarawy, B. Didier, T. D. Gibson and T. L. Windus, New Basis Set Exchange: An Open, Up-to-Date Resource for the Molecular Sciences Community, *J. Chem. Inf. Model.*, 2019, **59**, 4814–4820.

69 P. H. Willoughby, M. J. Jansma and T. R. Hoye, A guide to small-molecule structure assignment through computation of (^{1}H and ^{13}C) NMR chemical shifts, *Nat. Protoc.*, 2014, **9**, 643–660.